Image Cover Sheet

CLASSIFICATION	SYSTEM NUMBER
UNCLASSIFIED	511881

TITLE

Investigation of Plastic Zone Development in Dynamic Tear Test Specimens

System Number:

Patron Number:

Requester:

Notes: Paper # 7 contained in Parent sysnum #511874

DSIS Use only:

Deliver to: CL

Investigation of Plastic Zone Development in Dynamic Tear Test Specimens

T.S. Koko[1], J.R. Matthews[2], C.V. Hyatt[2] and V. Roy[2]

[1] Martec Limited, 400-1888 Brunswick Street, Halifax, N.S., B3J 3J8
[2]Dockyard Laboratory Atlantic, Defence Research Establishment Atlantic, P.O. Box 99000, Stn Forces, Bldg D17, Halifax, N.S., B3K 5X5

ABSTRACT

The J-integral is an elastic-plastic fracture criterion, which permits measurement of the fracture toughness of a specimen that has been fractured after general yielding. An understanding of the ratio of plastic zone size (radius) to the crack tip blunting (stretch zone) is required to determine the upper limit of temperature relative to full size transition curves where elastic plastic fracture becomes invalid. This study endeavours to acquire this ratio using finite element techniques. The development of the plastic zone in dynamic tear (DT) specimens and a non-standard three point bending fracture test specimen used to measure fracture properties was the main focus of the study. The ABAQUS finite element software was used to model the elastic-plastic behaviour of the specimens. For the DT specimen, a crack was induced by pressing the notch, followed by fatigue cracking at a limit load level of 40% of the specimen limit load, whereas, the crack shape for the non-standard specimen was a fatigue crack defined at approximately 30% of the limit load. The shapes of these cracks were adequately modelled in the finite element analysis. The specimens were made of 350WT steel and 304 stainless steel materials and were loaded until fixed amounts of permanent deformation were recorded. Results were obtained in the form of plots, showing the progression of the plastic zone around the crack tip. For each case, mid point plastic deflection, stretch zone width and plastic zone radius were computed. The finite element results obtained were compared to experimental elastic plastic testing where available, and reasonably accurate agreement was achieved.

INTRODUCTION

The J-integral is one of several criteria used to determine the fracture toughness of materials. This is a criterion that is suitable for measurement of fracture in the elastic-plastic regime of the full transition curve (Figure 1). It permits measurements of fracture toughness of specimens that have been fractured after general yielding, and assumes that onset of fracture is due to a critical level of stress or strain being achieved at or near the crack tip [1,2]. The J-integral is measured using three-point bend specimens, such as the dynamic tear (DT) test specimens. An understanding of the ratio of the plastic zone size (radius) to the crack tip blunting (stretch zone

width) is required to determine the upper limit of temperature relative to the full size transition curves where elastic-plastic fracture (J-integral) becomes invalid.

Figure 2 shows a typical DT specimen and Figure 3 shows idealizations of the plastic zone around the crack tip. As shown in Figure 3, the plastic zone radius is the maximum extent of the plastic zone, and the stretch zone width (SZW) is the distance from the crack tip to the interface of the plastic zone with the side of the crack. The shear lip size is given by the distance from the yield surface to the original surface on the side of the specimen. The standard validity criterion stipulates that

$$a, b, B = 50J / \sigma_{flow} \tag{1}$$

This suggests that B should be greater than $50J/\sigma_{flow}$. But blunting is approximately $J/(2\sigma_{flow})$. Therefore the thickness B should be greater than 100 times the critical blunting for a valid test. Thus, if the ratio (β) of plastic zone size to blunting size is known, then the following relations will hold for a valid fracture test:

$$\begin{aligned} B &> 100SZW \\ B &> 100r_y / \beta \\ B &> 100s / \beta \ (or\ s < B\beta/100) \end{aligned} \tag{2}$$

where r_y (plastic radius) = s (shear lip size) [3,4,5], $\beta = r_y/SZW$, and the flow stress σ_{flow} is given by $\sigma_{flow} = (\sigma_y+\sigma_u)/2$, where σ_y is the yield stress and σ_u the ultimate stress. Accordingly, in the present study, the key is to identify the ratio of plastic zone size to stretch zone width. Four methods of verification are available:

(i) Analytical (after Rice[6], who suggested the ratio was as low as 5 and as high as 600);
(ii) Visual (after experiments on stainless steel at DREA);
(iii) Experience in valid J testing (after DREA investigations); and
(iv) By finite element (looking at plastic deformation of the center of the bar, stretch zone or blunting, plastic zone, and the parameter *s* which actually includes the shear lip and lateral contraction).

The focus of this study is to utilize the finite element methodology to investigate the plastic zone development in three point bend fracture specimens. The aim of the study is to provide an understanding of the ratio of the plastic zone size (radius) to crack tip blunting (stretch zone width), in order to be able to predict the upper limit where elastic plastic fracture becomes invalid. Of interest is the investigation of the plastic zone development in standard dynamic tear (DT) test specimens with 350WT or 304 stainless steel materials; and a non-standard (NS) three-point bend specimen made of 304 stainless steel material.

PROBLEM DESCRIPTION

Geometry

A schematic representation of the test specimen is shown in Figure 2. In the present study, three test specimens are analyzed. These include the following:

(i) DT specimen with 350WT steel, designated as DT-350WT;
(ii) DT specimen with 304 stainless steel, designated as DT-304SS; and
(iii) Non-standard specimen with 304 stainless steel, designated as NS-304SS.

The DT specimens (DT-350WT and DT-304SS) had the following geometric properties: L=181 mm; S=164 mm; a=12 mm plus .010 inches pressing followed by fatigue extension of 13 to 20 mm; W=41 mm; and B=8 mm. The non-standard specimen had the following configuration: L=125 mm; S=100 mm; a=12.5 mm fatigue crack produced by rigorous process; W=25 mm; and B=12.5 mm, where L=length of beam; S=span of beam between supports; W=width of beam; B=thickness of beam; and a=notch size (fatigue sharpened).

Crack Tip Shape

The crack tip shape is that of a fatigue crack initially and a blunted fatigue crack thereafter. For the DT specimen the notch is first machined with an included angle of 60° followed by a pressing process that extends the notch 0.254 mm (0.010) with an included angle of 40° and a resulting crack tip radius of 0.254 mm (0.001). This is followed by fatigue cracking at a load level of no more than 40% of the current specimen limit load. This produces a sharp fatigue crack of definable dimensions, which is used in the FE simulation. This pre-cracking extends the pressed notch by at least 1 mm. The crack tip shape for the non-standard specimen is that of a well established fatigue crack whose maximum loading has been defined by careful laboratory fatiguing (maximum load approximately 30% of the limit load). The shape of the resulting crack tip and the configuration of the crack along its entire length were acquired by sectioning. Detailed descriptions of the precracking process are available in Reference [7].

FINITE ELEMENT MODEL

Finite Element Approach

The prediction of the response behaviour of the DT specimen requires a tool that accounts for large geometry changes and plasticity effects in the crack tip region. There are several commercial FEA tools that can be employed or adapted for calculating the stresses and strains needed. In this study the ABAQUS finite element software [8] was used to model the elastic-

plastic behaviour of the DT specimen. The software has a wide range of non-linear material models and can account for large strains and displacements. Moreover, it has been successfully used for the analysis of similar problems [9-11]. However, the HyperMesh [12] general-purpose pre- and post-processing program was used for model generation and results processing.

Finite Element Meshes

As stated, the HyperMesh code was used to generate the finite element models of the DT and non-standard specimens, which were then translated to ABAQUS input files. The exact shapes of the crack were obtained from DREA to enable accurate modelling of the structural configuration. Figure 4 shows the shape of the fatigue crack in the DT specimen. This shape had to be modelled accurately to provide meaningful results. Detailed 2-D finite element models of the specimen were developed. In order to reduce the problem size only one-half of the structure was modelled. The finite element models of the DT and non-standard (NS) specimens are as shown in Figures 5 and 6, respectively. Plane strain elements were used to model the structure. These elements allow for the treatment of large displacements, finite strains and plasticity, which are expected to occur in the specimen.

Material Models

An incremental rate independent plasticity theory available in the ABAQUS finite element program [8] was used for the material constitutive model. This standard model for plasticity is summarized here for completeness. The total multi-axial strain state ε_{ij}, expressed in terms of elastic and plastic components is given by

$$\in_{ij} = \in^{e}_{ij} + \in^{p}_{ij} \tag{3}$$

The total logarithmic uniaxial strain, ε, consistent with the integration of the rate of deformation tensor for a multiaxial strain state, is decomposed as

$$\in = \in^{e} + \in^{p} \tag{4}$$

where $\in^{e}, \in^{p}$ are the elastic and plastic strain vectors, respectively. The yield function f is related to uniaxial tension by

$$f(\tau_{ij}) = \tau(\in^{p}), \tag{5}$$

where τ_{ij} and τ are the multiaxial Kirchoff and uniaxial stress states, respectively. The von Mises yield criterion and an associated flow rule is used for the incremental analysis, where the von Mises yield function is given by

$$f(\tau_{ij}) = \left(\frac{3}{2}(S_{ij}S_{ij})\right)^{1/2}, \tag{6}$$

where S_{ij} is the deviatoric component of stress. The Kirchoff stress and logarithmic strain measures are employed because of computational convenience. The Kirchoff stress tensor, τ_{ij}, is approximately equal to the Cauchy stress tensor, σ_{ij}, for deformations involving only small changes in volume [10,11]. This condition is assumed in the elastic-plastic analysis. The

uniaxial Cauchy stress-logarithmic strain constitutive relations of the material are input, in multilinear form, as Cauchy stress and logarithmic plastic strain pairs for the ABAQUS program. The constitutive parameters for the 350WT and 304SS materials are described below.

350WT Steel

The material for the first DT specimen was 350WT steel. The engineering stress-strain curve for this material was obtained from DREA. This curve terminated at a strain of 25%. However, from experimental investigations by DREA [13], strains as high as 250% were observed around the crack tip of the specimen. A method for defining the stress-strain behaviour beyond 25% strain was therefore required. Two possible stress-strain curves, as illustrated in Figure 7, were considered. In the first model (Figure 7(a)), the stress was assumed to be constant at the maximum stress level from 25% to 250% strain. This case is referred to as the flat curve model. In the second constitutive model (Figure 7(b)), the stress was assumed to rise from the maximum uniaxial test stress of about 600 MPa to 1100 MPa from 25% to 250% strain. The maximum stress value was determined from experimental observation and intuition [13]. This second case is referred to as the rising curve model.

304 Stainless Steel

The second DT specimen and the non-standard specimens were made of 304 stainless steel material. The stress strain curve for the material was obtained from the literature [14]. This curve terminated at a strain of about 80%. However, from experimental investigations by DREA [13], strains as high as 1000% were observed around the crack tip of the specimen. In this case only the rising curve model was used beyond the 80% strain level. The possible stress-strain curve is illustrated in Figure 8. In this constitutive model the stress was assumed to rise from the maximum uni-axial test stress of about 600 MPa to 1000 MPa from 80% to 1000% strain. The maximum stress value was determined from experimental observation and intuition [13].

Boundary Conditions and Loading

The following boundary conditions were applied:

At the support:	$v = 0$
Along the center line:	$u = 0$;

Where, u,v are the displacements components in the longitudinal and transverse directions. The load was applied as a concentrated load at the top middle point of the beam.

RESULTS AND DISCUSSIONS

The finite element results obtained for the three specimen configurations are discussed in this section. For each specimen, results of the midpoint displacement, plastic zone development and stretch zone width are provided.

DT Specimen with 350 WT Steel Material

Midpoint Displacements

The predicted load-displacement response of the midpoint of the beam is shown in Figure 9. In the figure, DL refers to the displacement of the top midpoint with respect to the top left end point, and DS refers to the bottom midpoint with respect to the support point. The results obtained from using the flat and rising stress-strain curves are all presented in the figure. It is seen that the use of a flat or rising stress-strain curve does not have any significant effect on the midpoint displacement responses. The applied load has been non-dimensionilized with respect to the limit load P_L, which is given by

$$P_L = \frac{4}{3}\left(\frac{Bb^2\sigma_y}{S}\right) \tag{7}$$

where B is the thickness, b is the untracked ligament (b=W-a), σ_y is the yield strength and S is the span between the supports.

Plastic Zone Development

The shape of the plastic zone was similar for both the flat and rising stress-strain models. However, the stress and strain levels beyond the 25% strain level were quite different for the two cases because of the different load paths. Figure 10 shows the development of the von Mises stresses and equivalent plastic strains in the DT-350WT material with the rising curve model, at different load levels. For the von Mises stress plots, all regions with stresses above the yield stress of 450 MPa are shown in red, and the area that has not yielded is shown in blue. For the equivalent plastic strain plots, all areas with plastic strains greater than 0.01% are shown in red and all other areas are shown in blue. Also, the same view is used for all the figures so a direct comparison of the shape and size of the plastic zone can be made. It is seen that the shapes and size, of the plastic zones using the von Mises stress or equivalent plastic strain are very similar. Also, as expected, the plastic zone size increased with load. In addition, the plastic zone tends to rise upwards from the tip of the crack, which is similar to the experimentally observed behaviour [2].

Figure 11 shows the plastic zone that has strained over 15% (when necking starts) of two load levels. In comparison with the plastic zones at the corresponding load levels in Figure 11, it is seen that necking occurs in only a small area around the crack tip.

Plastic Zone Radius (r_y) Stretch Zone Width (SZW) and Ratio r_y/SRW
The plastic zone radius, r_y, and the stretch zone width (SZW) at various load levels were measured from the plastic zone configurations. The plastic zone was given by the distance from the crack tip to the farthest point of the plastic zone. The stretch zone width (SZW) was given by the distance from the crack tip to the interface of the plastic zone with the side of the crack (see Figure 3). Figures 12 and 13 respectively show the variation of the plastic radius and SZW with load, for the flat and rising stress-strain curve models of the DT-350WT specimen. The figures show that the plastic zone radii and stretch zone widths obtained from the two models are almost identical as for the shapes of the plastic zones, as discussed above. The ratios of the plastic zone radius to stretch zone width (r_y/SZW) were also computed and presented in Figure 14. Again, the responses from the two constitutive models are very similar, and the ratios vary from 50 to 90. Due to the fact that the configurations of the plastic zone predicted by the flat and rising curve constitutive models were similar, only the rising curve (strain hardening) model was used for the remaining specimens, as this provided more realistic strain levels.

DT Specimen with 304 Stainless Steel Materials

Midpoint-Displacement
The predicted load-displacement response of the midpoint of the beam is shown in Figure 15. The displacements of the DT-304SS specimen are smaller than those of the DT-350WT specimen. For instance, at $1.1P_L$, the midpoint displacement with respect to the end point, DL, is approximately equal to 0.3mm compared to 0.63mm for the DT-350WT specimen (see Figure 9), since the applied load for the DT-304SS specimen (7.49 kN) was less than the load applied to the DT-350WT specimen (16 kN).

Plastic Zone Development
Figure 16 shows the development of the von Mises stresses in the DT-304SS specimen. In the plots, all regions with stress above the yield stress of 240 MPa are shown in red and the area that has not yielded is shown in blue. As before, the same view is used for the plots to facilitate direct comparison. The plastic zone configurations at various load levels follow the same pattern as described for the DT-350WT specimens. The area around the crack tip that was strained by more than 15% was insignificant.

Plastic Zone Radius (r_y), Stretch Zone Width (SZW) and Ratio r_y/SZW
The plastic zone radius and SZW at various loads were measured as described above. Figure 17 shows the variation of plastic radius with load. For comparison, the plastic zone radii of the DT-350WT specimen are also shown. As shown, the plastic radii for the DT-304SS specimen follow the same trend as for the DT-350WT specimen, and the plastic radii for the two specimens are very close, with those of the DT-304SS specimen being slightly larger. Figure 18 shows the variation of SZW with load. Again, the trends of the results for the DT-304SS and DT-350WT specimens are similar. However, the values of the SZW for the DT-304SS specimen are generally smaller than those of the DT-350WT specimen. The variation of the ratio of the plastic

radius to the stretch zone width is shown in Figure 19, where a plot of the ratio for the DT-350WT specimen is also shown. Both ratios increase slightly with load, however, the range of the r_y/SZW for the DT-304SS specimen is 140-150 compared to 50-90 for the DT-350WT specimen, this is expected, since the 304SS material was more ductile than the 350WT steel.

NS Specimen with 304 Stainless Steel Material

Midpoint Displacement
The predicted load-displacement response of the midpoint of the beam is presented in Figure 20. The computed midpoint displacement of the last load step (1.044PL) was 0.18 mm compared to 0.23 mm obtained experimentally [7,15].

Plastic Zone Development
The predicted von Mises stresses and equivalent plastic strains at various load levels for the NS-304SS specimen are shown in Figure 21. The plastic zones are defined by the regions with stresses over 240 MPa or over 0.01% plastic strain. It is observed that the plastic zones predicted by using the stress or strain criterion are very similar. The same view is used for all the plots to facilitate direct comparison.

Plastic Zone Radius (r_y), Stretch Zone Width (SZW) and Ratio r_y/SZW
The variations of plastic zone radius and stretch zone with (SZW) with load, for the NS-304SS specimen are presented in Figures 17 and 18, respectively. For comparison, the corresponding results for the DT-350WT and DT-304SS specimens are also shown in the figures. It is observed that the plastic radius and SZW for the NS-304SS specimen are generally smaller than those of the DT-350WT and DT-304SS specimens. The variation of the ratio of plastic radius to stretch zone width is shown in Figure 19 along with the corresponding results for all the other specimens. The r_y/SZW ratio for the NS-304SS specimen fall generally between those of the DT-350WT and DT-304SS specimens.

SUMMARY, CONCLUSIONS AND RECOMMENDATIONS

This paper focussed on a study to investigate plastic zone development in three point bend fracture specimen. The finite element methodology was utilized to provide an understanding of the plastic zone size (radius) to crack tip blunting (stretch zone width), in order to be able to predict the upper limit where elastic plastic fracture becomes invalid. Finite element analysis of three test specimen configurations were performed. The test specimens were (i) a standard dynamic tear (DT) test specimen with 350WT steel; (ii) another standard DT specimen with 304 stainless steel; and (iii) a non-standard three point bend specimen with 304 stainless steel. The ABAQUS finite element code was used to perform incremental elastic-plastic analysis of the specimens. Intuition and experimental observation were used to develop approximate stress-strain curves for the materials beyond the points where uniaxial stress-strain data were available

for the 350WT steel and 304 stainless steel materials.

The results computed for each analysis included the midpoint displacement; development of the plastic zone around the crack tip with progression of load; the plastic zone radius r_y; stretch zone width (SZW); and the ratio of plastic zone radius to SZW. The results were presented in the form of contour plots and charts for comparison with experiments being performed concurrently. It was found that the plastic zone radius r_y and stretch zone width SZW increased parabolically with load, up to 1.1 P_L, where P_L is the limit load. On the other hand, the variation of the ratio r_y/SZW with load fitted a linear distribution for all cases. This ratio was found to vary from 50-90 for the DT specimen with 350WT steel; 140-150 for the DT specimen with 304 stainless steel and 90 -140 for the non-standard specimen with 304 stainless steel.

The experimental results were not fully available to this study, as they were being performed concurrently. It is recommended that the results of this study be compared to the experimental results when they are available. Based on these comparisons it might be necessary to refine the stress-strain relations beyond the points where uniaxial test data available, to obtain better accuracy. Once a good level of accuracy has been achieved with the finite element model, it is further recommended that the analysis be applied to several other specimen configurations to enable a parametric study to be performed. Such a study would lead to the generation of generalized charts that can be used for fracture measurements and design.

REFERENCES

[1] Matthews, J.R. Porter, J.F. and Hyatt, C.V. "Fracture Control for Submarine Pressure Hulls II." 3rd Meeting of the TTCP PTP1 Operating Assignment on Fracture Control of Naval Structures, Annapolis, Maryland 1-3 May 1991.

[2] Matthews, J.R., Porter, J.F., Hyatt, C.V. and KarisAllen, K.J. "A General Discussion of Short Crack Fracture." proceedings of the Conference on Shallow Crack Fracture Mechanics Tests and Applications, Cambridge UK, 23-24 Sept, 1992.

[3] Matthews, J.R., Hyatt, C.V., Porter, J.F., and KarisAllen, K.J. "Effect of Thickness On The Relationship Between Shear Lip and Energy In Dynamic Tear Specimens", Engineering Fracture Mechanics, Vol 60, No.5-6, August 1998.

[4] Matthews, J.R. "On The Relationship Between Shear Lip, Shear Index and Energy In Dynamic Tear Specimens", Engineering Fracture Mechanics, 31 May 1996.

[5] Matthews, J.R., "On The Relationship Between Shear Index and Energy in Dynamic Tear Specimens," Engineering Fracture Mechanics, Vol 39, No.1, 1991.

[6] Rice, J.R. in Journal of Applied Mechanics Series E of Transactions of the ASME,

Vol., 90, June 1968.

[7] Roy, V. Hyatt, C.V. and Matthews, J.R. "Precracking Stainless Steel 304 for Notch Tip Plastic Zone Studies." DREA Note No. DL(A)/98/1, 1998.

[8] Hibbitt, H.D. Karlsson, B.I. and Sorensen, E.P. ABAQUS User's Manual, 1990.

[9] DeGiorgi, V.G., Kirby III, G.C. and Jones, M.I. "Prediction of Classical Fracture Initiation Toughness." Engineering Fracture Mechanics, Vol. 33, No. 5, pp. 773-785, 1989.

[10] DeGiorgi, V.G. and Matic, P. "A Computational Investigation of Local Material Strength and Toughness on Crack Growth." Engineering Fracture Mechanics, Vol. 39, No. 5, pp. 1039-1058, 1990.

[11] DeGiorgi, V.G., Matic, P., Bar-on, I. and Lee, G.M.C. "An Experimental and Computational Investigation of Crack Growth Initiation in Three-Point Bend Fracture Specimens." Engineering Fracture Mechanics, Vol. 50, No. 1, pp. 1-9, 1995.

[12] HyperMesh User's Manual.

[13] Matthews, J.R. Private comunications, 1999.

[14] Boyer, H.E. Atlas of Stress-Strain Curves. ASM International, Metals Park, Ohio.

[15] Koko, T.S., Gallant, B.K. and Tobin, S.B. "Investigation of Plastic Zone Development in Dynamic Tear Test Specimens", Martec Report TR-99-16, June 1999.

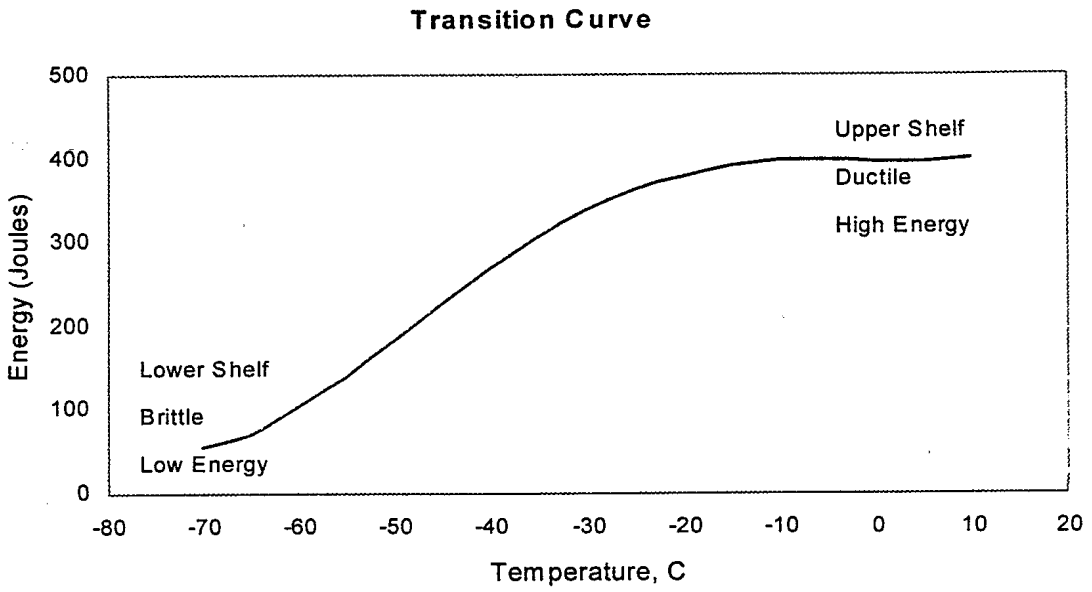

Figure 1: Typical Transition Curve

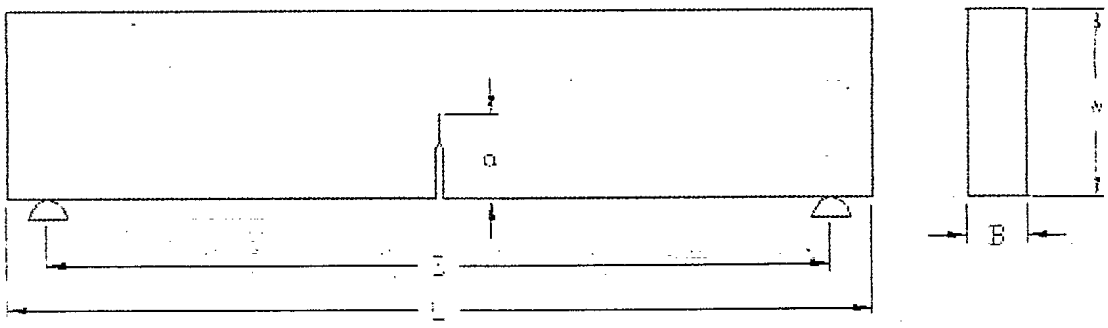

Figure2: Configuration of DT Specimen

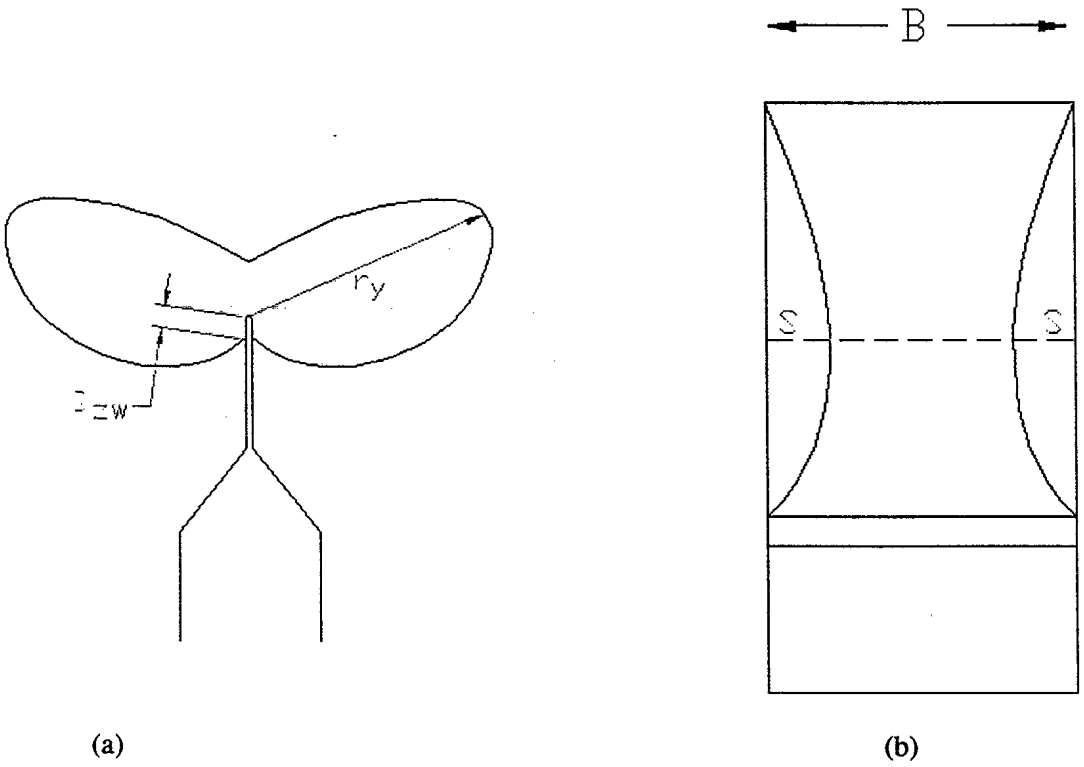

Figure 3: Idealization of Plastic Zone around Crack Tip

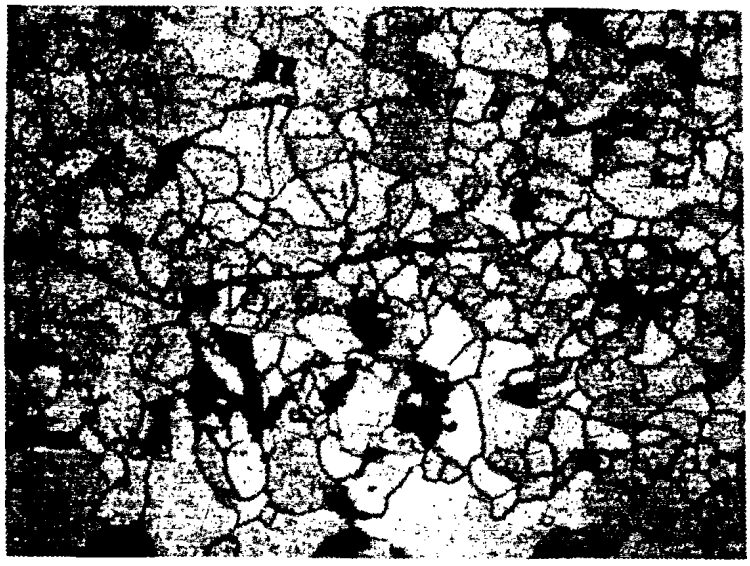

Figure 4: Shape of Fatigue Crack in DT Specimens

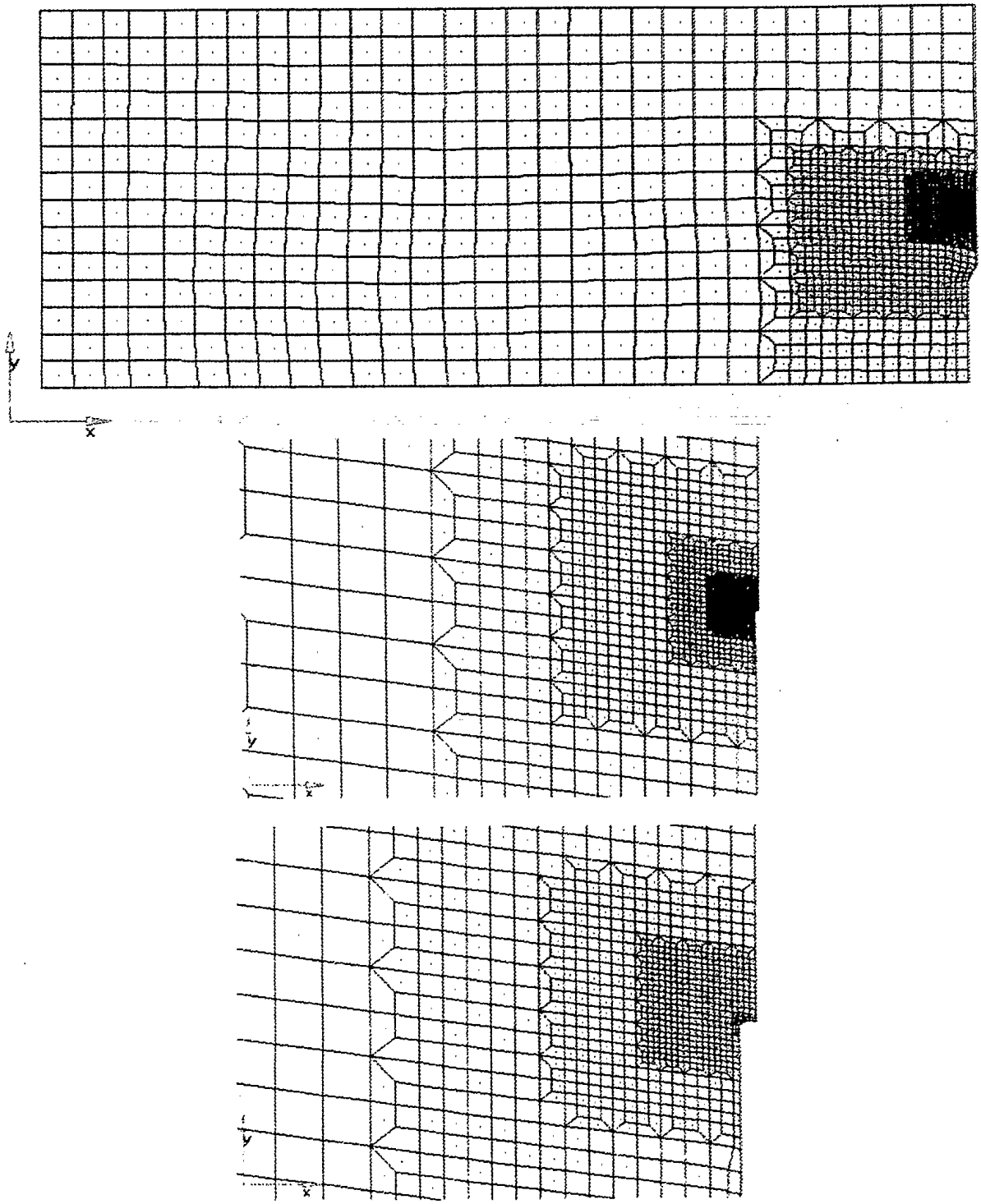

Figure 5: FE Mesh of DT Specimens

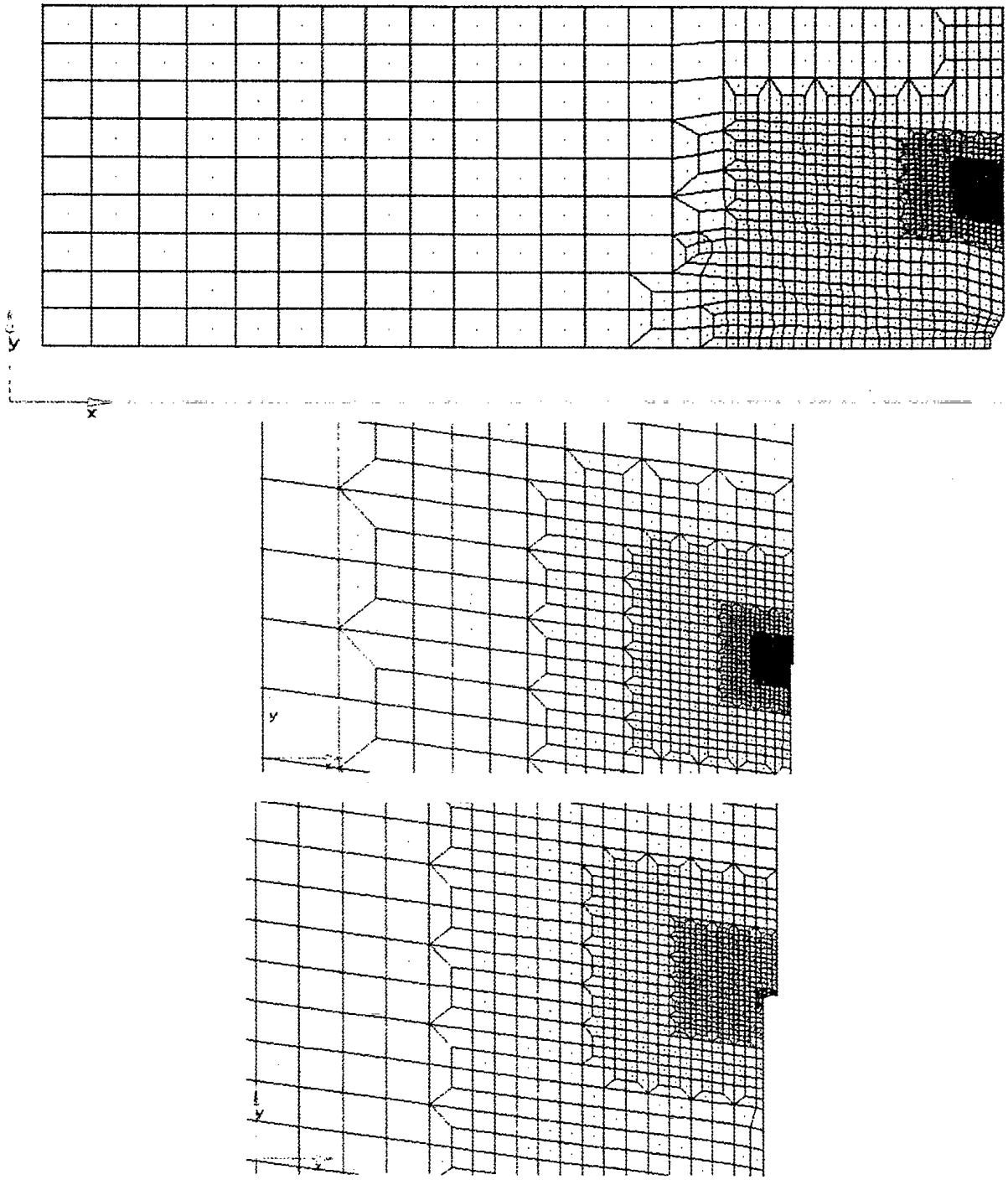

Figure 6: FE Mesh of Nonstandard (NS) Specimens

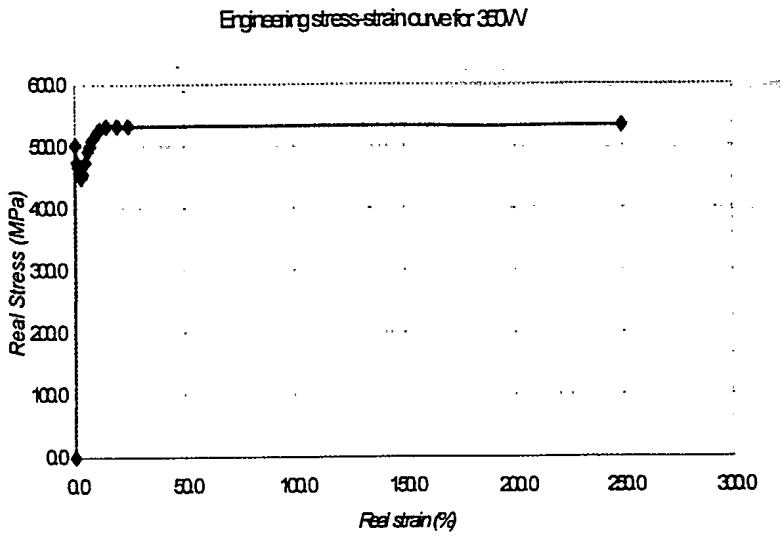

(a)

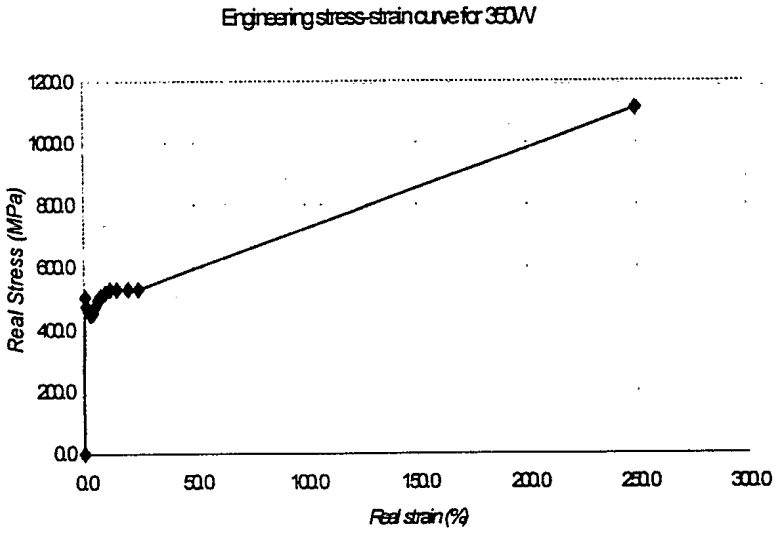

(b)

Figure 7: Stress-Strain Curves for 350WT Steel

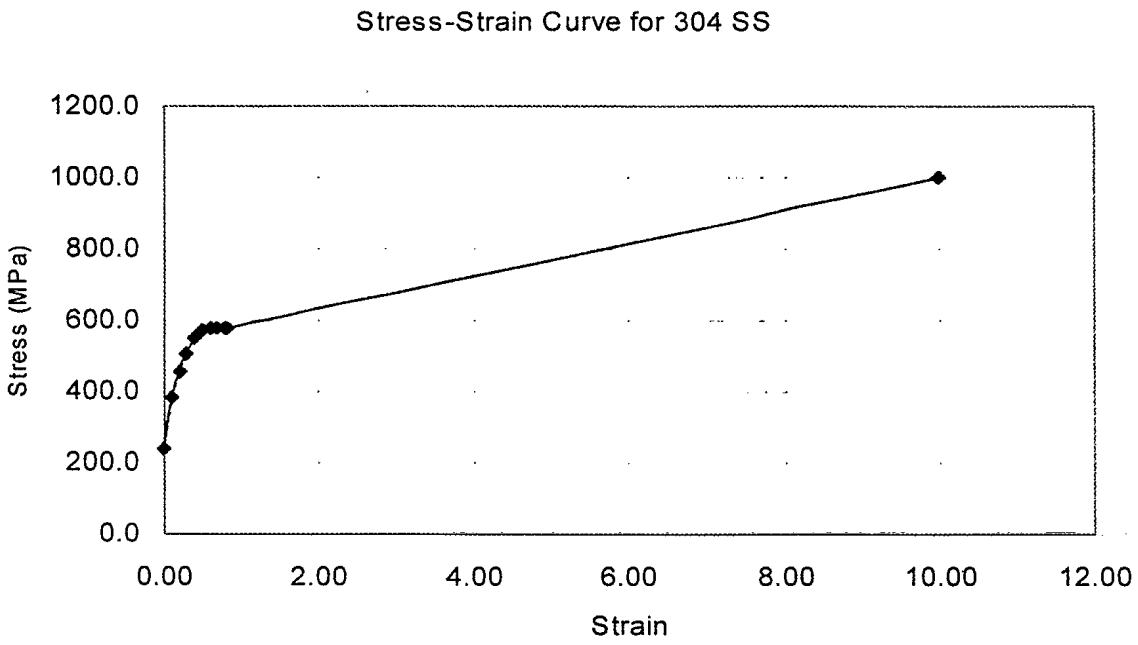

Figure 8: Stress-Strain Curves for 304 Stainless Steel

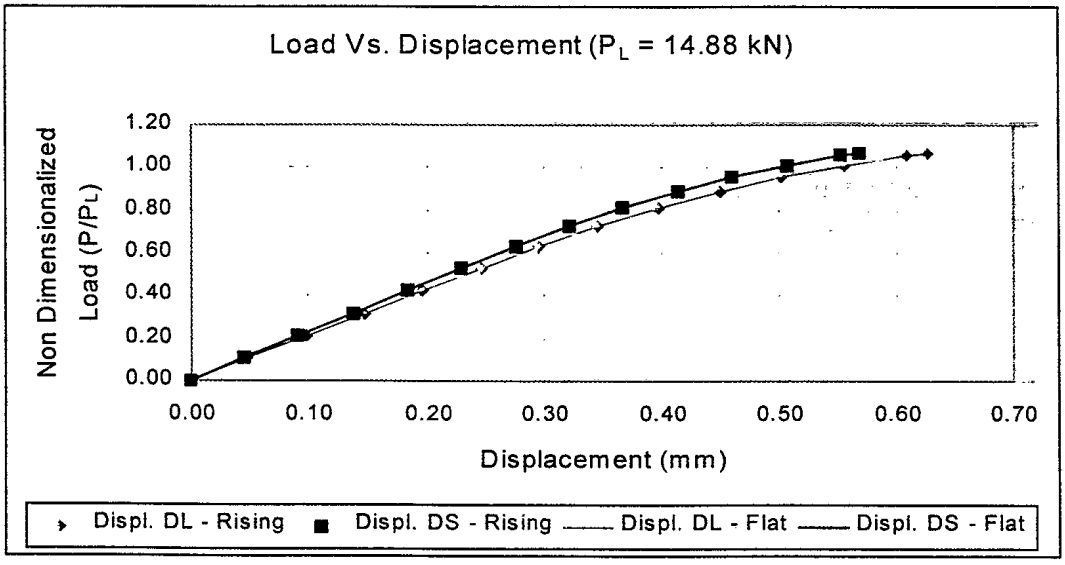

Figure 9: Midpoint Displacement Responses of DT-350WT Specimen, with Flat and Rising Stress-Strain Curve Models

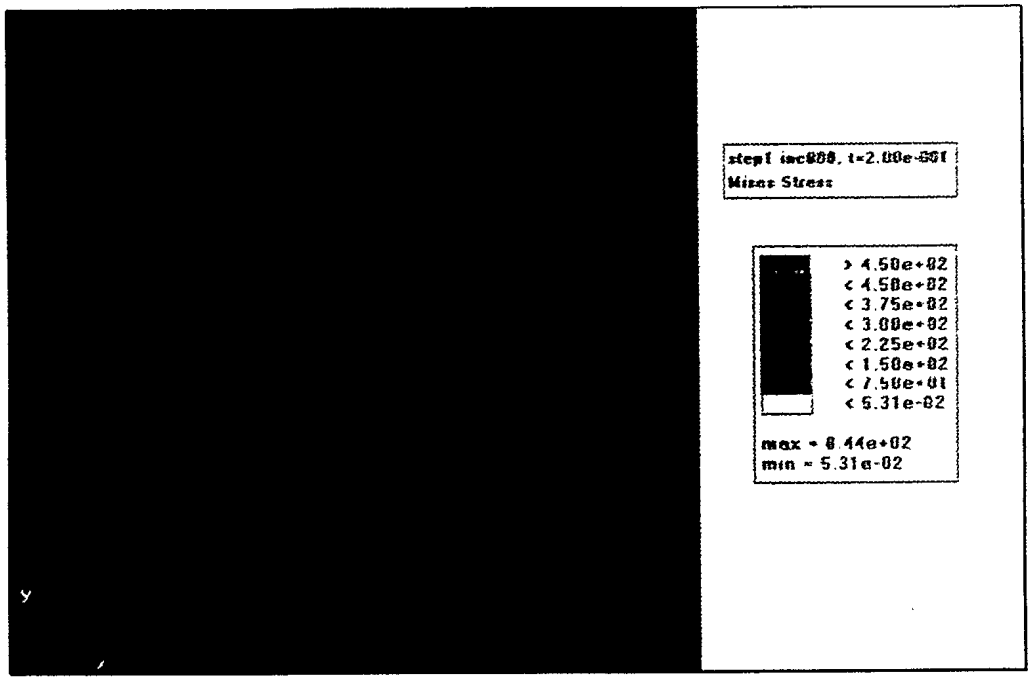

(a)

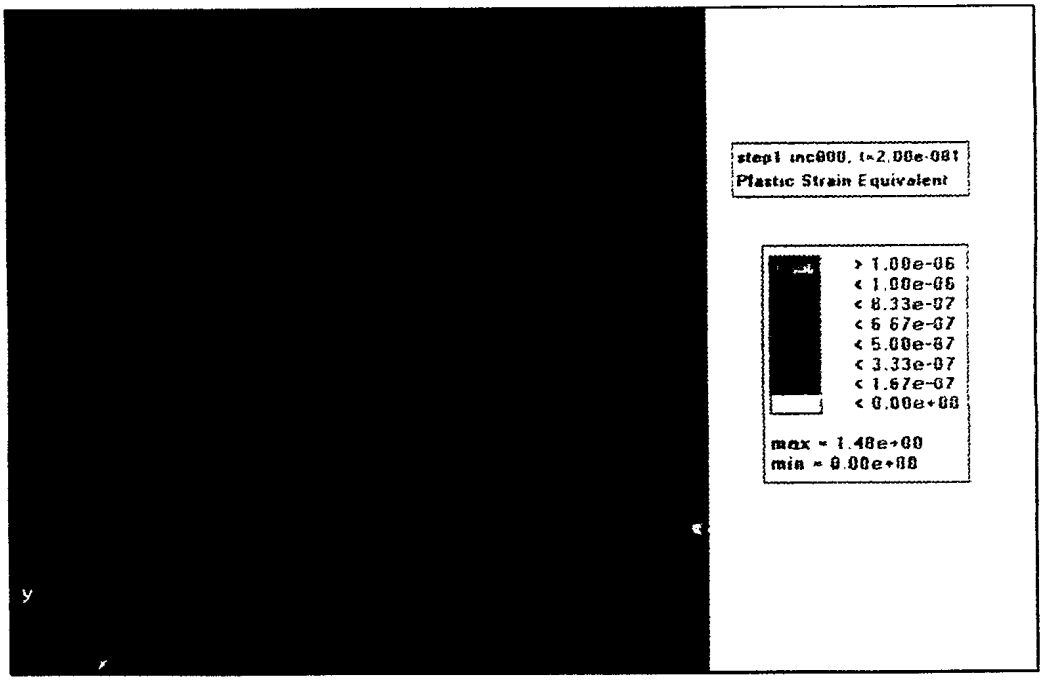

(b)

Figure 10: von Mises Stress and Equivalent Plastic Strain Development, in DT-350WT Specimen with Rising Stress-Strain Curve Model
(a) von Mises Stress and (b) Plastic Strain at 3.19 kN (0.21 P_L)

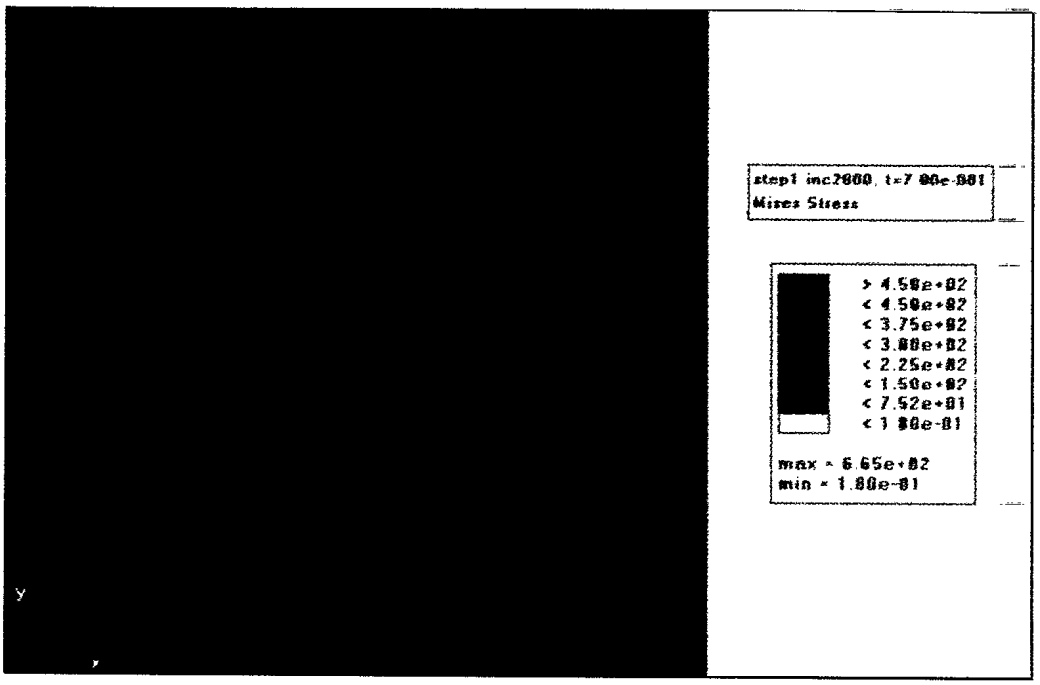

(c)

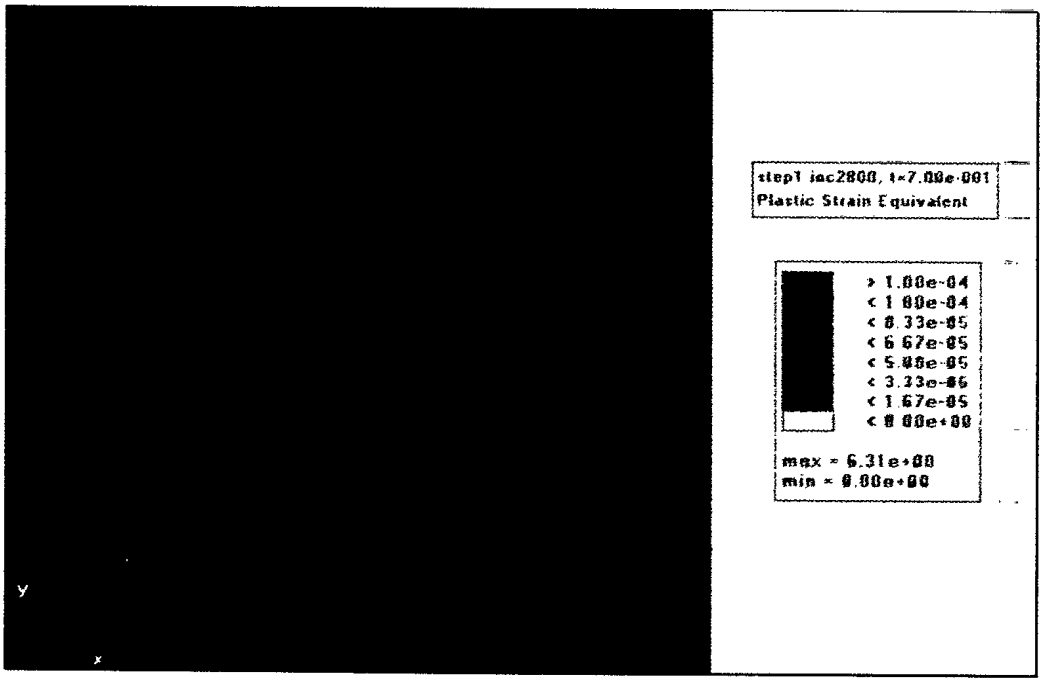

(d)

Figure 10 Continued: von Mises Stress and Equivalent Plastic Strain Development, in DT-350WT Specimen with Rising Stress-Strain Curve Model
(c) von Mises Stress and (d) Plastic Strain at 10.81 kN (0.73 P_L)

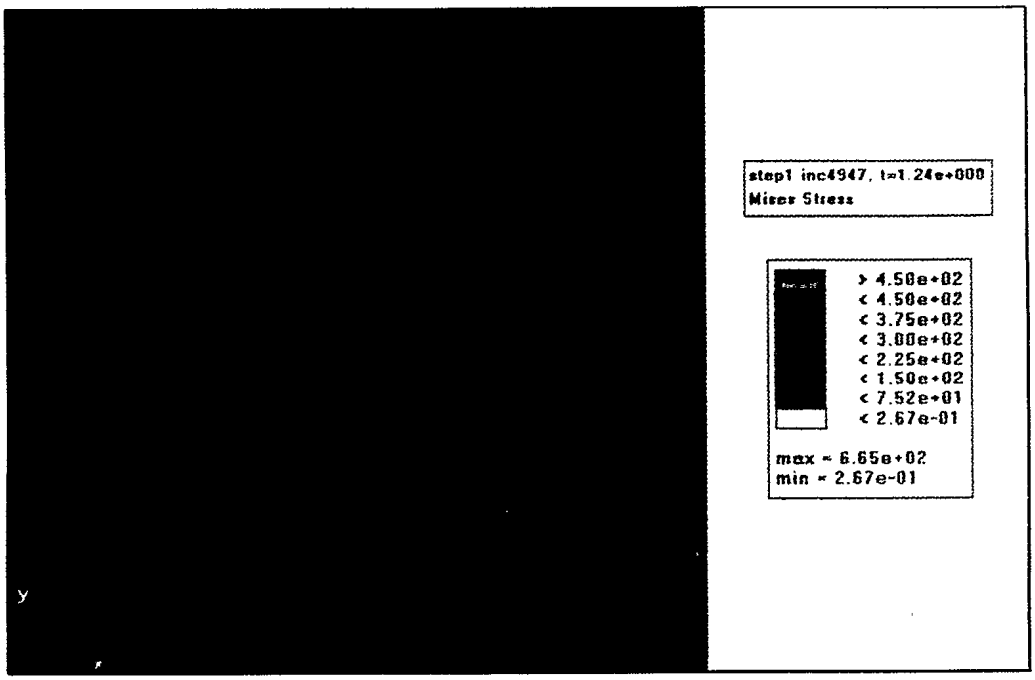

(e)

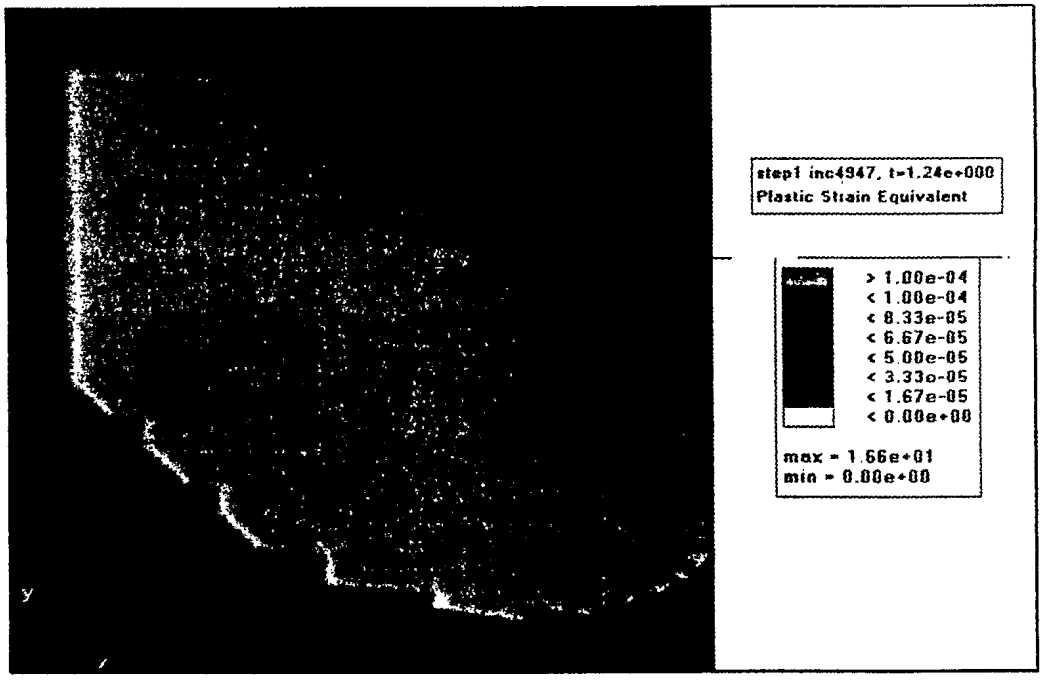

(f)

Figure 10 Continued: von Mises Stress and Equivalent Plastic Strain Development, in DT-350WT Specimen with Rising Stress-Strain Curve Model
(e) von Mises Stress and (f) Plastic Strain at 16.00 kN (1.08 P_L)

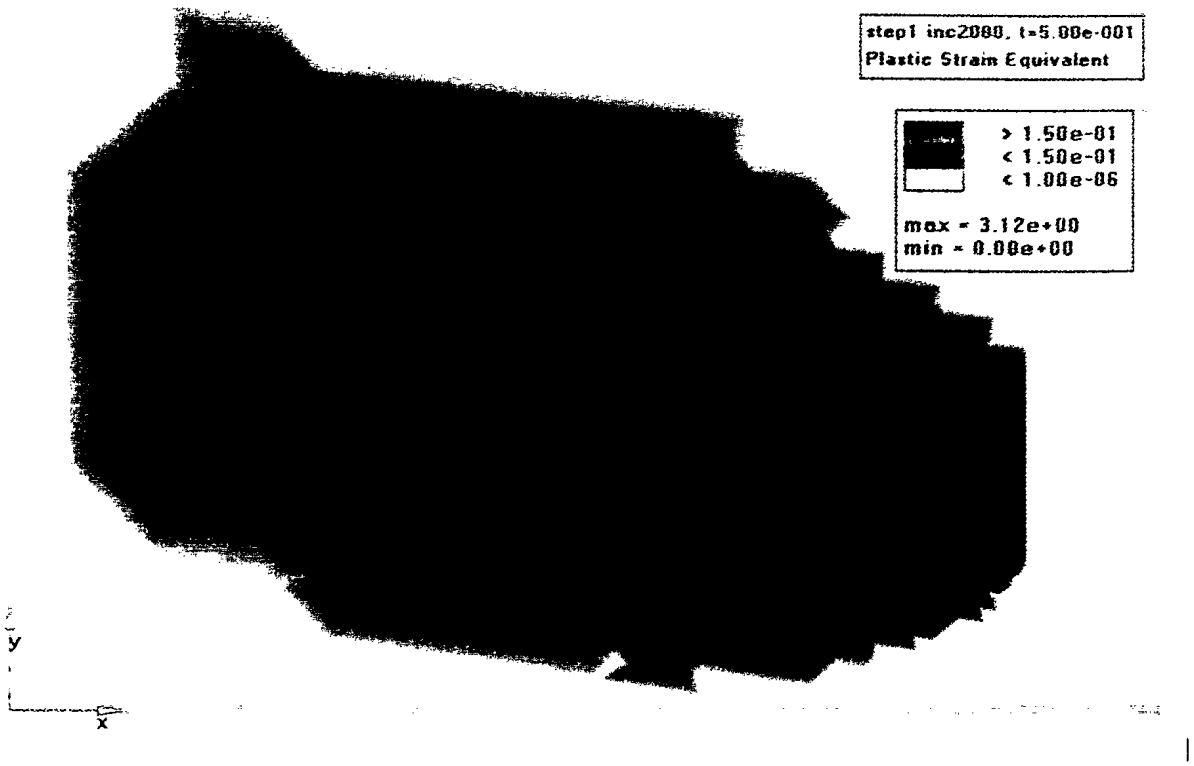

Figure 11: Plastic Zone Configuration of DT-350WT Specimen Showing Area with Greater than 15% Plastic Strain at 7.87 kN (0.53 P_L)

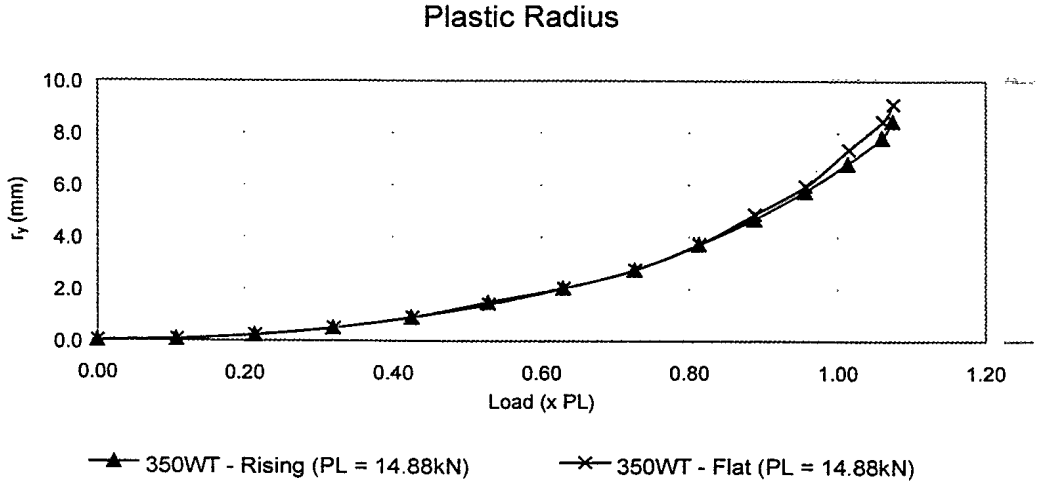

Figure 12: Plastic Radius of DT-350WT Specimen

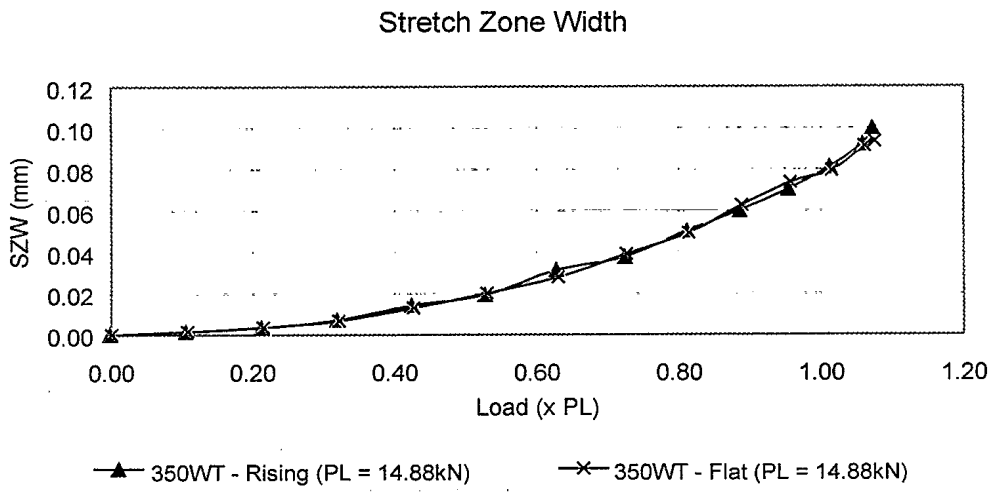

Figure 13: Stretch Zone Width of DT-350WT Specimen

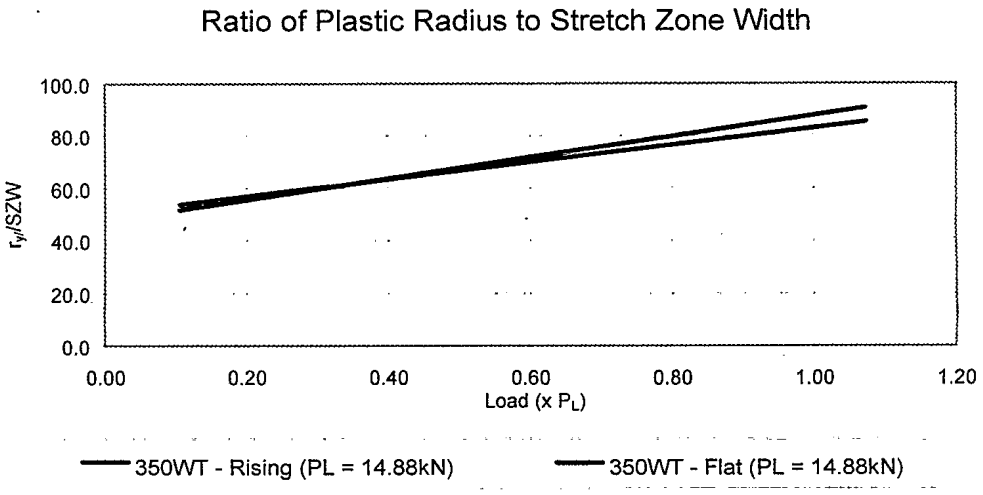

Figure 14: Ratio of Plastic Radius to Stretch Zone Width of DT-350WT Specimen

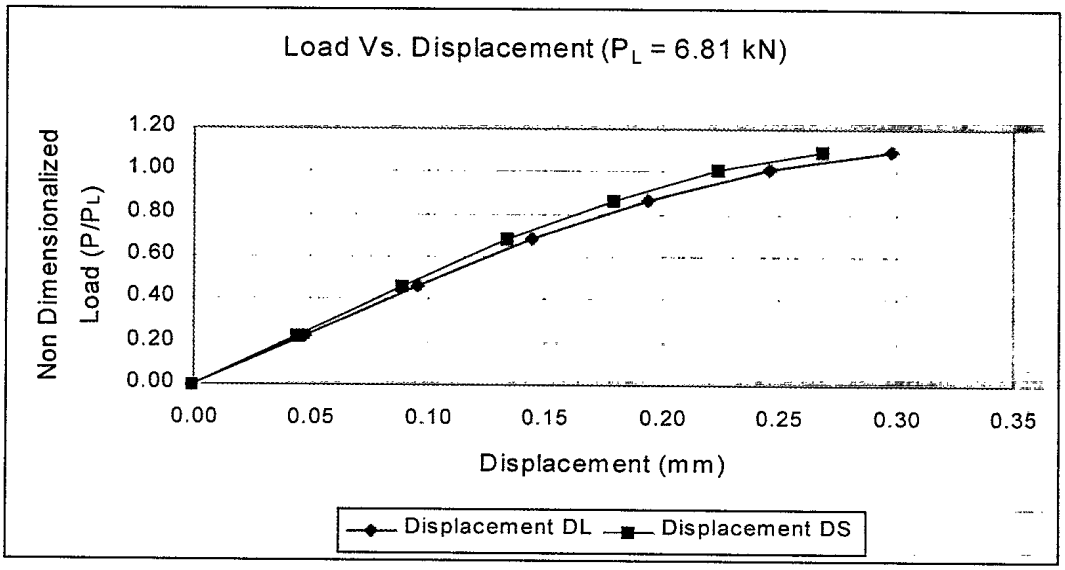

Figure 15: Midpoint Displacement Response of DT-304SS Specimen, Rising Curve Model

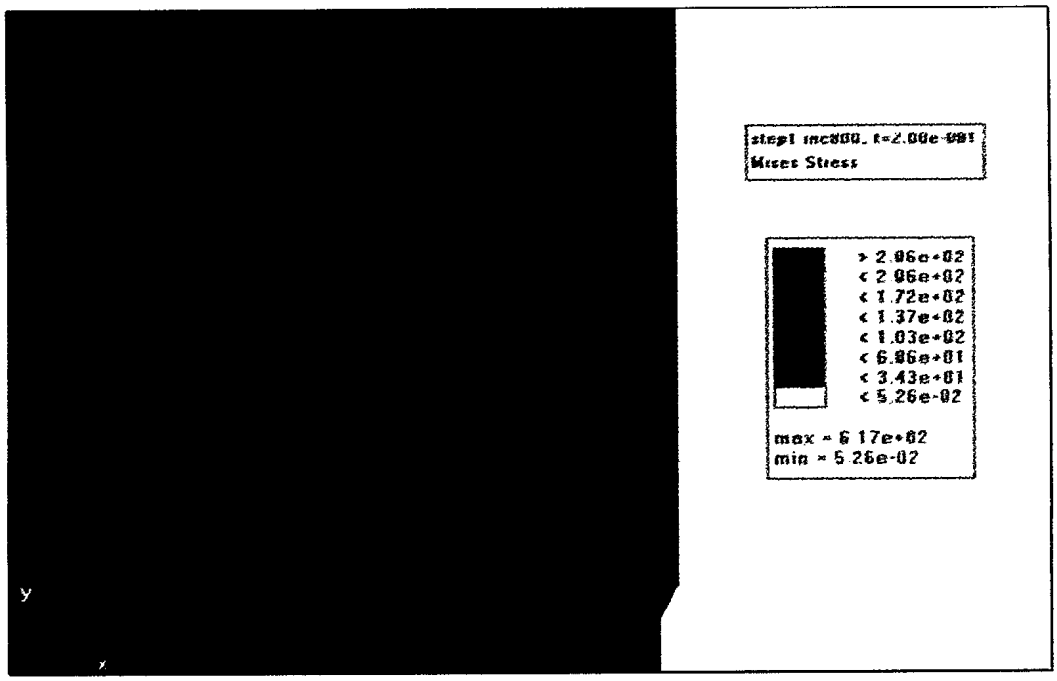

(a)

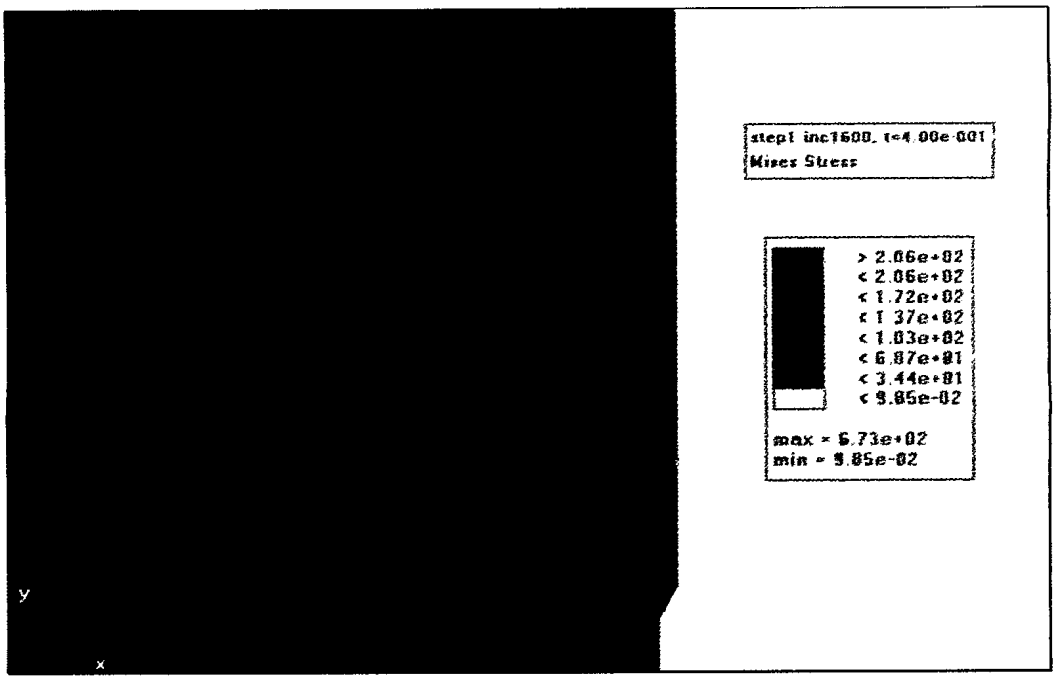

(b)

Figure 16: von Mises Stress Development in DT-304SS Specimen with Rising Stress-Strain Curve Model: (a) at 3.16 kN (0.46 P_L) and (b) at 5.92 kN (0.87 P_L)

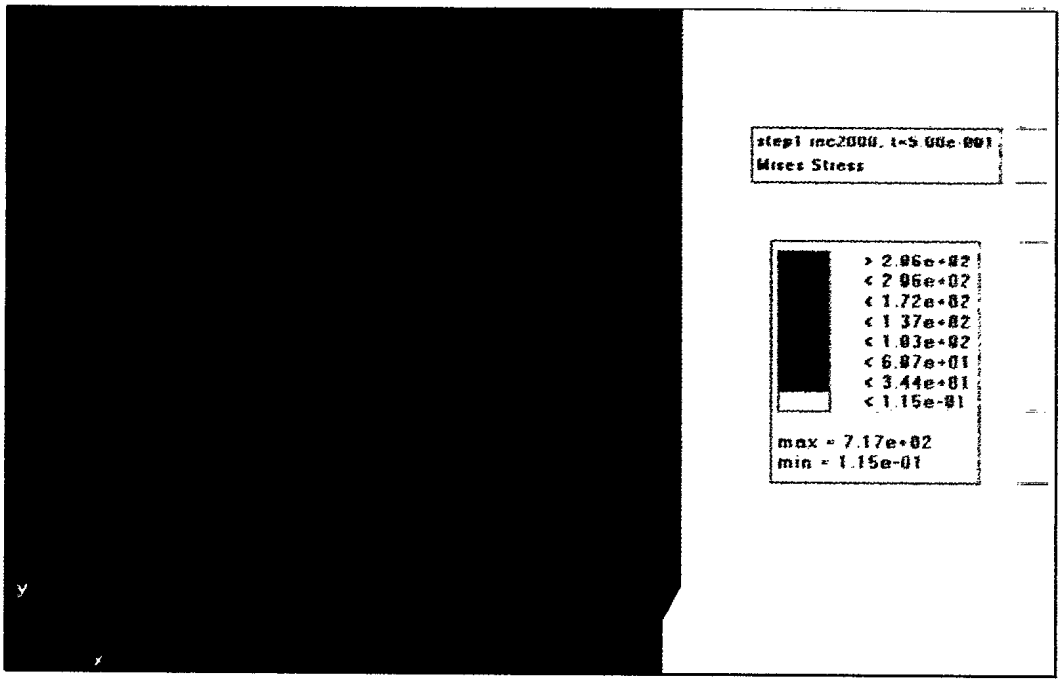

(c)

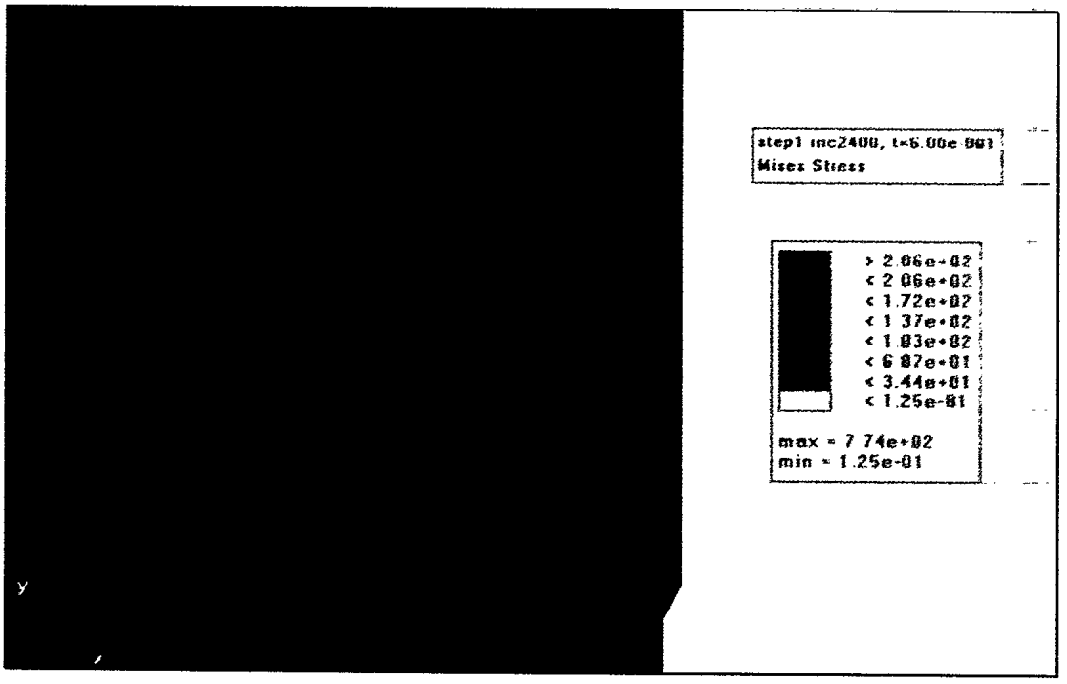

(d)

Figure 16 Continued: von Mises Stress Development in DT-304SS Specimen with Rising Stress-Strain Curve Model: (c) at 6.88 kN (1.01 P_L) and (d) at 7.48 kN (1.10 P_L)

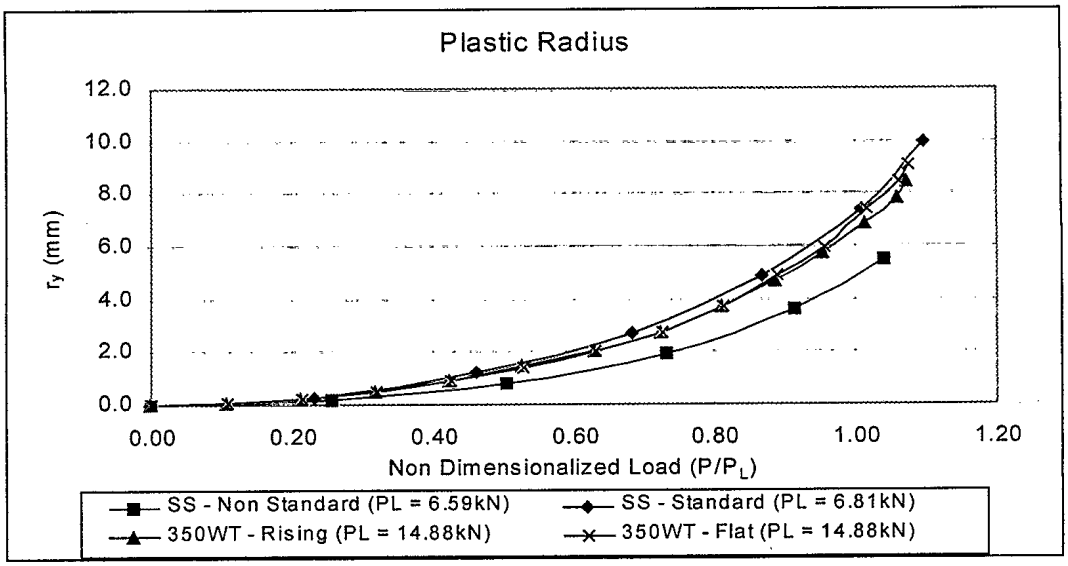

Figure 17: Comparison of Plastic Zone Radius

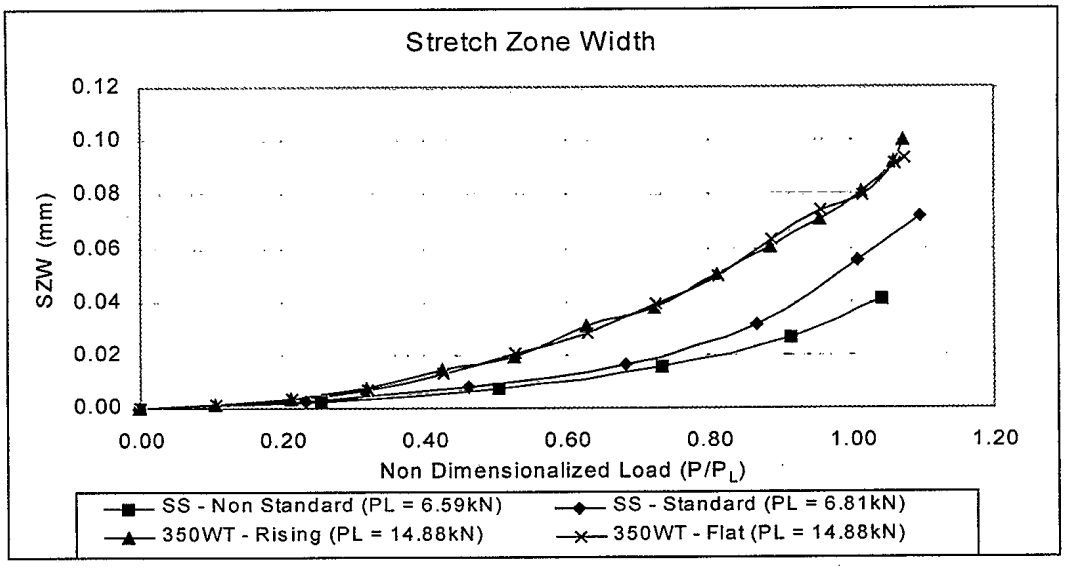

Figure 18: Comparison of Stretch Zone Width

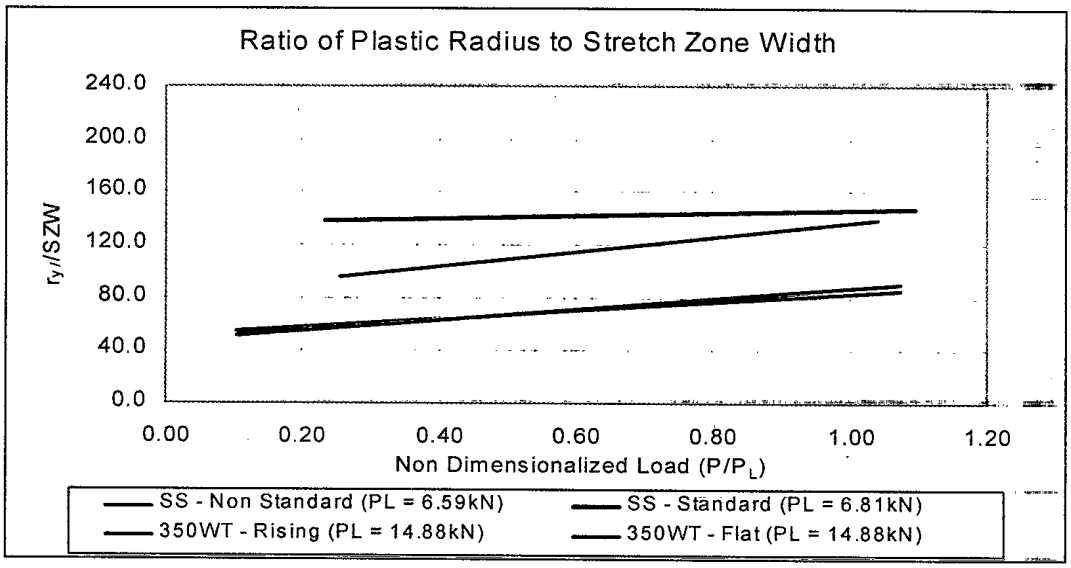

Figure 19: Comparison of Plastic Radius to Stretch Zone Width

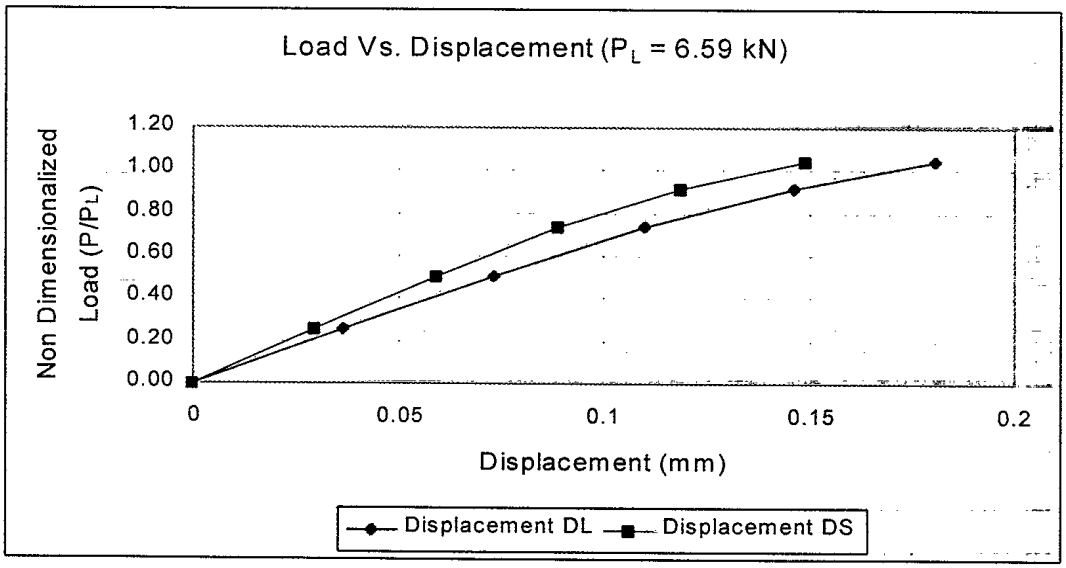

Figure 20: Midpoint Displacement Response of NS-304SS Specimen With Rising Stress-Strain Curve

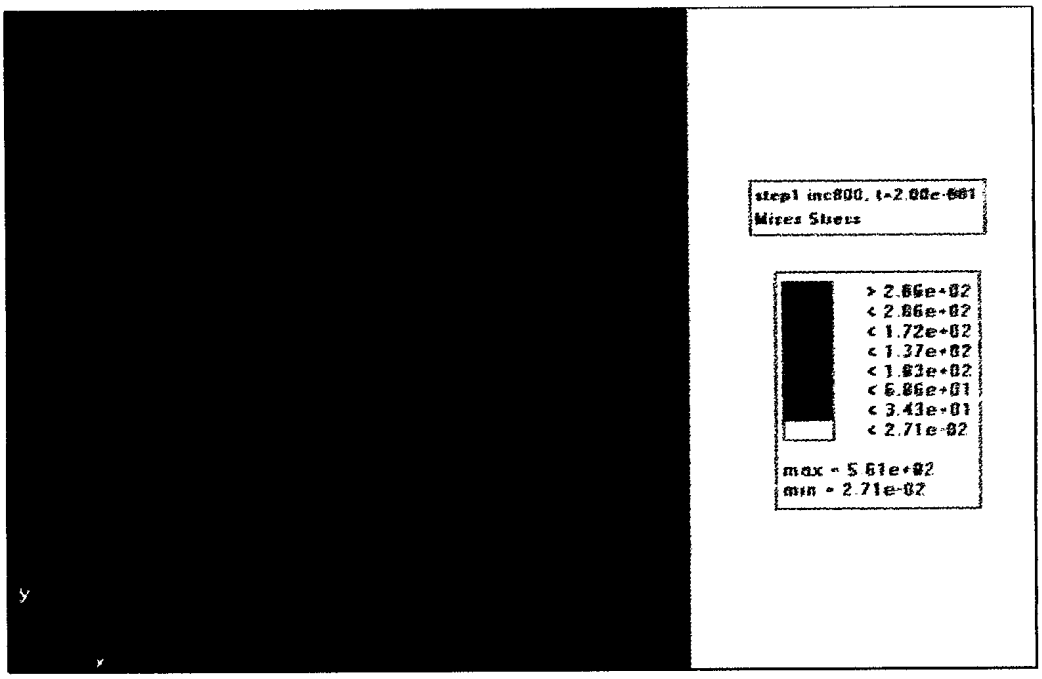

(a)

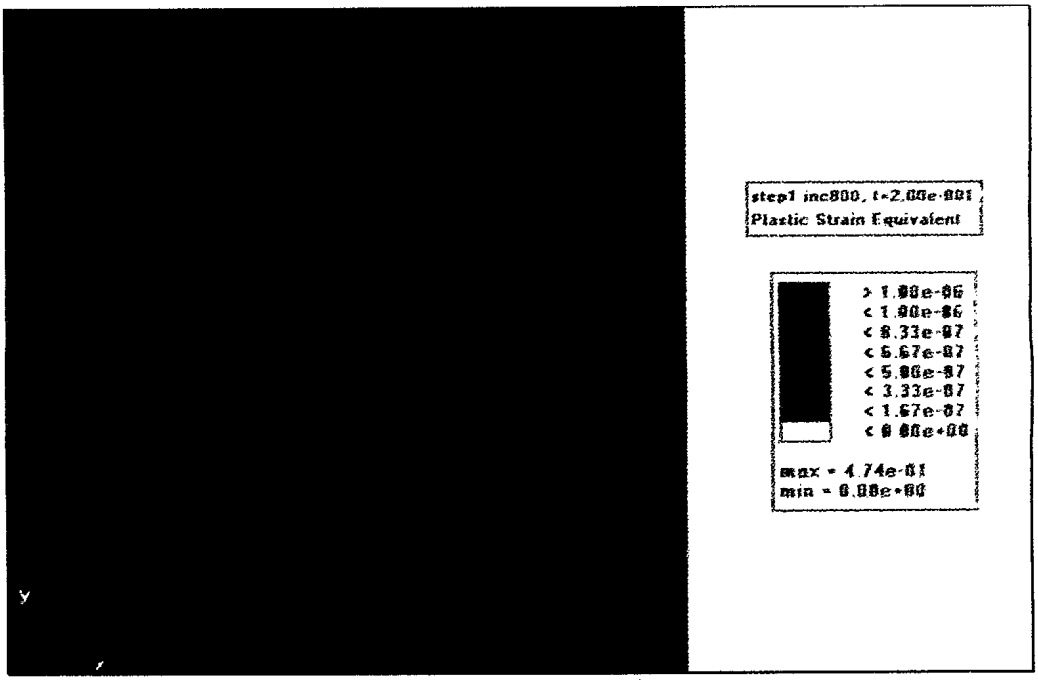

(b)

Figure 21: Plastic Zone Configurations of NS-304SS Specimens With Rising Stress-Strain Curve Model: (a) von Mises Stress and (b) Plastic Strain at 1.69 kN (0.26 P_L)

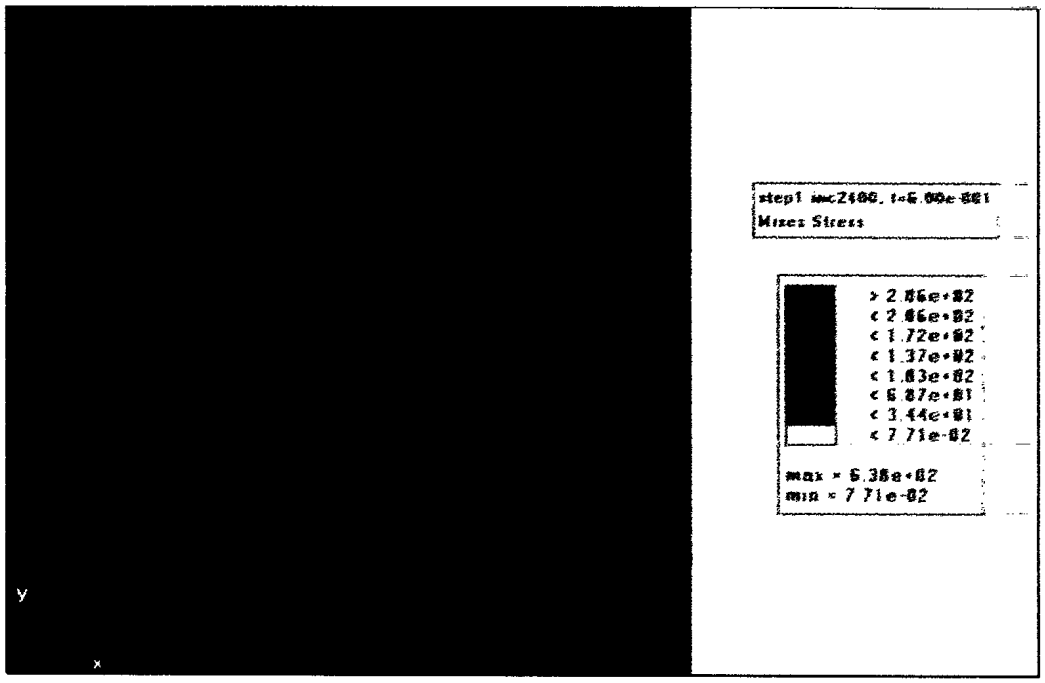

(e)

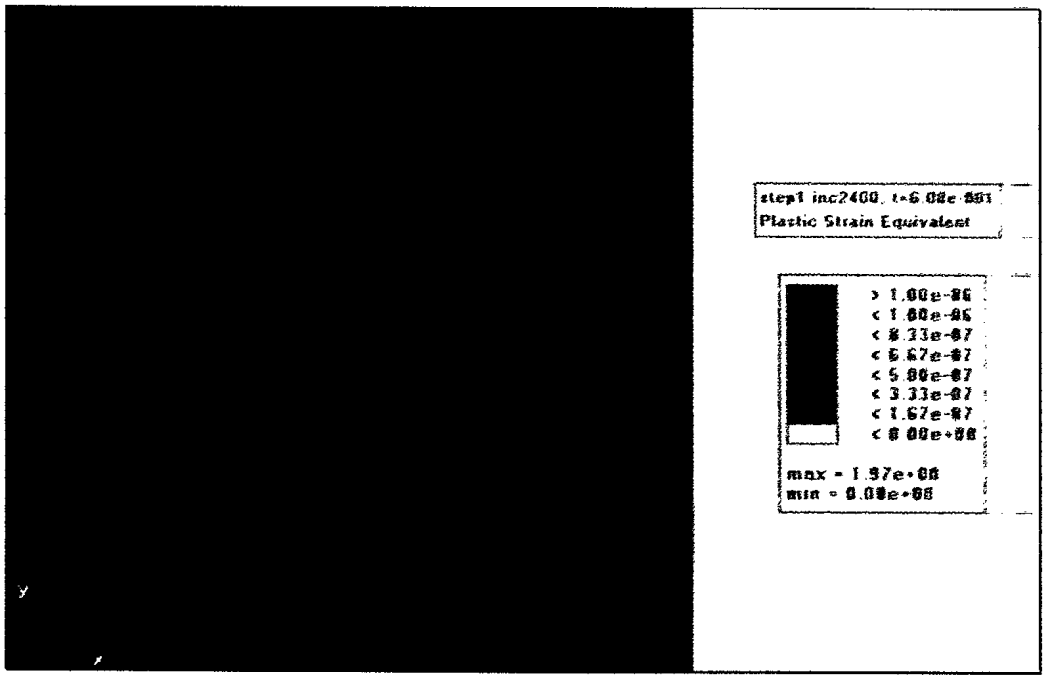

(f)

Figure 21 Continued: Plastic Zone Configurations of NS-304SS Specimens With Rising Stress-Strain Curve Model: (e) von Mises Stress and (f) Plastic Strain at 4.85 kN (0.74 P_L)

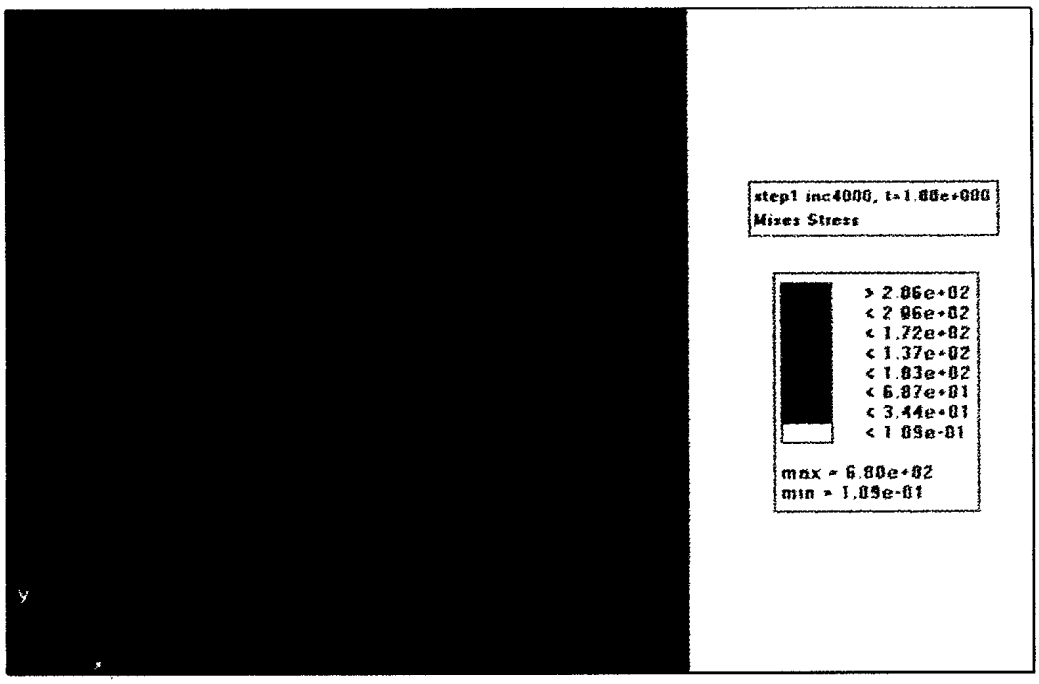

(i)

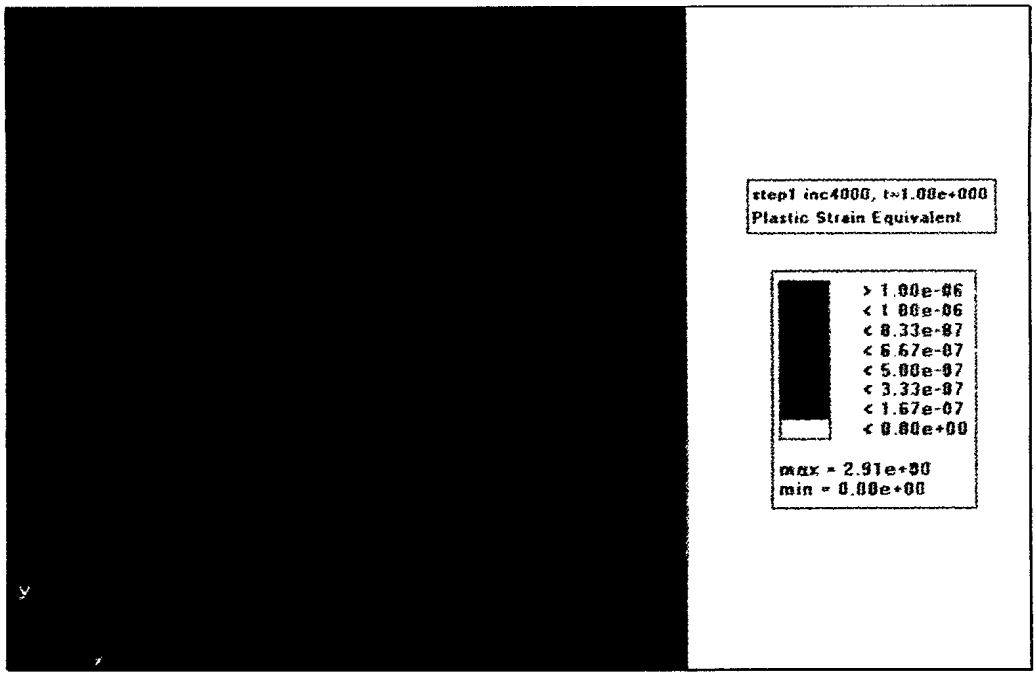

(j)

Figure 21 Continued: Plastic Zone Configurations of NS-304SS Specimens With Rising Stress-Strain Curve Model: (i) von Mises Stress and (j) Plastic Strain at 6.88 kN (1.04 P_L)